Coherence of a dynamically decoupled single neutral atom

Chang Hoong Chow,[1] Boon Long Ng,[1] and Christian Kurtsiefer[1,2]

[1]*Center for Quantum Technologies, 3 Science Drive 2, Singapore 117543*
[2]*Department of Physics, National University of Singapore, 2 Science Drive 3, Singapore 117542*[*]

(Dated: July 24, 2020)

Long qubit coherence and efficient atom-photon coupling are essential for advanced applications in quantum communication. One technique to maintain coherence is dynamical decoupling, where a periodic sequence of refocusing pulses is employed to reduce the interaction of the system with the environment. We experimentally study the implementation of dynamical decoupling on an optically-trapped, spin-polarized ^{87}Rb atom. We use the two magnetic-sensitive $5S_{1/2}$ Zeeman levels, $|F = 2, \ m_F = -2\rangle$ and $|F = 1, \ m_F = -1\rangle$ as qubit states, motivated by the possibility to couple $|F = 2, \ m_F = -2\rangle$ to $5P_{3/2}$ the excited state $|F' = 3, \ m'_F = -3\rangle$ via a closed optical transition. With more refocusing pulses in the dynamical decoupling technique, we manage to extend the coherence time from $38(3)\,\mu s$ to more than two milliseconds. We also observe a strong correlation between the motional states of the atom and the qubit coherence after the refocusing, which can be used as a measurement basis to resolve trapping parameters.

I. INTRODUCTION

Quantum memories for efficient retrieval of a photonic qubit and long-lived storage are important building blocks for future applications of quantum communication [1, 2]. Strong light-atom interaction is essential to accomplish a substantial information exchange between photons and atomic systems, or to implement an atom-mediated interaction between flying photonic qubits [3]. One approach to realize such a quantum interface considers strong focusing of the optical mode onto a confined atom [4–8].

In our experiment, we optically trap a single neutral atom at the focus of a high numerical aperture lens for an incoming probe mode to achieve efficient light-atom coupling. The clean energy level structure of a neutral atom and the trapping in ultra-high vacuum permits deriving the interaction strength with minimal assumptions.

In this work, we probe the lifetime of a coherent superposition of the $5S_{1/2}$ ground state Zeeman levels, $|F = 2, \ m_F = -2\rangle \equiv |\uparrow\rangle$ and $|F = 1, \ m_F = -1\rangle \equiv |\downarrow\rangle$ as our qubit states. The $|\uparrow\rangle$ state can be coupled to an auxiliary state $5P_{3/2}$, $|F' = 3, \ m' = -3\rangle$ via a closed optical transition, opening a possible path to protocols originally developed for solid state quantum systems to be implemented in an atomic system. This includes schemes for the generation of time-bin atom-photon entanglement and the sequential generation of an entangled photonic string [9, 10], which are crucial resources for quantum computations.

However, dephasing could lead to loss of information, reducing the fidelity of these entangled states. In comparison to other qubit configurations for neutral atoms, our interface based on the stretched states is more susceptible to noise such as magnetic field fluctuations. In earlier experiments, we have shown that a linearly polar-

———————
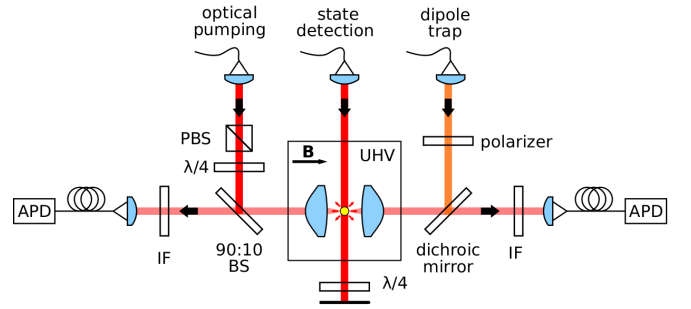[*] christian.kurtsiefer@gmail.com

FIG. 1. Setup for probing light-atom interaction in free space. APD: avalanche photodetectors, UHV: ultra-high vacuum chamber, IF: interference filter centered at 780 nm, $\lambda/2$: half-wave plate, $\lambda/4$: quarter-wave plate, PBS: polarizing beam splitter, BS: beam splitter, B: magnetic field.

ized dipole trap can significantly reduce atomic motion-induced qubit dephasing without impacting the light-atom coupling [11]. One approach to further suppress decoherence is to apply dynamical decoupling (DD) techniques [12–19].

We demonstrate that DD is efficient in mitigating the dephasing of the atomic qubit. The experimental setup and the state readout procedure is described in Sec. II. We first characterize our qubit system by performing Rabi spectroscopy (Sec. III), and carry on with applying various types of DD (Sec. IV). From the result, we analyze the dephasing mechanisms and tailor the refocusing sequence such that the coherence is optimally preserved (Sec. V).

II. EXPERIMENTAL SETUP

Our experiment starts with a single ^{87}Rb atom trapped in a red-detuned far off-resonant dipole trap (FORT) that is loaded from a magneto-optical trap (MOT). This dipole trap is formed by a linearly polarized Gaussian

laser beam (wavelength 851 nm) that is tightly focused by a pair of high numerical aperture lenses (NA = 0.75, focal length $f = 5.95$ mm) to a waist of $w_0 = 1.4\,\mu$m [11, 20]. Part of the atomic fluorescence is collected through the same lenses and coupled into single mode fibers that are connected to avalanche photodetectors (APD).

Once an atom is trapped, we apply 10 ms of polarization gradient cooling to reduce the atomic motion to a temperature of 14.7(2) μK [21]. Our dipole trap has an axial trap frequency ω_a of around $2\pi \times 12$ kHz, which corresponds to a mean axial vibrational mode number n_z of 25 with $(n_z + 1/2)\hbar\omega_z = k_B T$. This implies that the atom is not close to its motional ground state. Then, a bias magnetic field of 1.44 mT is applied along the FORT laser propagation direction to remove the degeneracy of the Zeeman states, and the atom is optically pumped into $5S_{1/2}\,|F = 2, m_F = -2\rangle \equiv |\uparrow\rangle$. We implement a lossless state-selective detection method [22, 23] by sending light resonant to the $5S_{1/2}$, $F = 2$ to $5P_{3/2}$, $F' = 3$ transition onto the atom for 600 μs and collecting the fluorescence light from the atom within this time window. The atomic state can be inferred from the photodetection events recorded at the APDs.

The detection fidelity is characterized by first preparing the atom in a particular state and then performing a state detection. When the atom is prepared in the $|\uparrow\rangle$ state, the detectors record a mean of photon number $n_\uparrow = 11.7(1)$. For atom in the $|\downarrow\rangle$ state, we expect the atom to scatter almost no photons due to the hyperfine splitting of 6.8 GHz. However, we find that in the experiment, the detectors occasionally register one or two events during the detection window (mean of photon number $n_\downarrow = 0.36(1)$).

We repeat this procedure for 2800 times. The histogram of $n_\uparrow$ and $n_\downarrow$ is shown in Figure 2. From this histogram, we can choose a threshold photon number n_{th} that maximizes the discrimination between the two states. Using $n_{th} = 3$, the probabilities of a state assignment error are $\xi_\uparrow = 4.4(4)\%$ and $\xi_\downarrow = 0.8(2)\%$ for atoms prepared in states $|\uparrow\rangle$ and $|\downarrow\rangle$, respectively. With this, we achieve a detection fidelity of $F = 1 - (\xi_\uparrow + \xi_\downarrow)/2 = 97.4(2)\%$.

III. RABI SPECTROSCOPY

Atoms in the $|\uparrow\rangle$ state are coupled to $|\downarrow\rangle$ by applying a microwave field resonant to this transition using a pair of log-periodic antennae. We then use this field to drive Rabi oscillations and perform Ramsey and various dynamical decoupling sequences to characterize the atomic coherence [24–28]. The Rabi oscillation in Figure 3 (top), exhibits a Rabi frequency of $\Omega_{mw} = 2\pi \times 76.78(3)$ kHz with a visibility of 0.837(7). The maximum visibility is related to state detection fidelity through $V_{max} = 1 - 2(1 - F)$, so V_{max} of 0.948(4) can be achieved assuming there is no other sources of error. Rabi oscillation shows little decay within the first 60 μs, implying that the re-
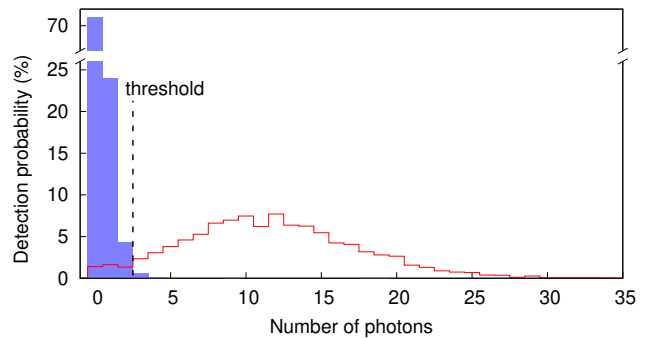

FIG. 2. Histogram of photon detection probability for atoms prepared in $F = 1$, $|\downarrow\rangle$ (blue) and $F = 2$, $|\uparrow\rangle$ (red) of the ground state manifold, respectively.
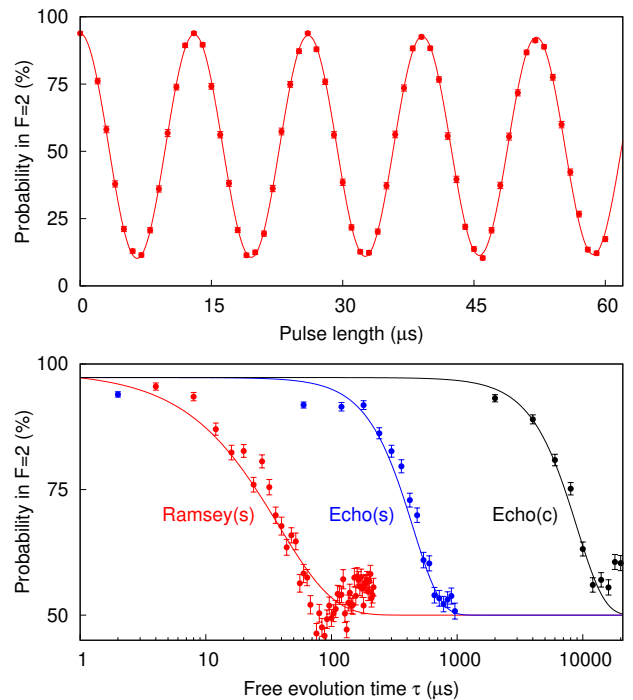

FIG. 3. Top: Rabi oscillation between $|\uparrow\rangle$ and $|\downarrow\rangle$. Solid line is a fit to an exponentially decaying cosine function to extract the Rabi frequency, $\Omega_{mw} = 2\pi \times 76.78(3)$ kHz. Bottom: Ramsey and spin-echo when the atom is initially prepared in $|\uparrow\rangle$ (s) or $|F = 2, m_F = 0\rangle$ (c). We fit a decaying exponential to the Ramsey signal and a decaying Gaussian to the spin-echo signal to extract their respective $1/e$ time constants; $T_{2,s}^* = 38(3)\,\mu$s, $T_{2,s} = 480(21)\,\mu$s, and $T_{2,c} = 9.5(6)$ ms.

duced visibility is most likely due to imperfections in the state preparation process. As shown in Figure 3(top), the probability of the atom in $F = 2$ does not go near to zero implies that there is a non-zero probability that the atom is in other Zeeman states that do not couple to the microwave field.

To determine the dephasing time of the qubit system, we carry out a Ramsey experiment where we apply two

$\pi/2$-pulses ($t_{\pi/2} = \pi/(2\Omega)$) with a free evolution time τ in between the two pulses to the atoms in the $|\uparrow\rangle$ state. We repeat the experiment for different τ and fit an exponential decay to the Ramsey contrast, which results in dephasing time $T_2^* = 38(3)\,\mu$s [Fig. 3 (bottom)].

Next, we apply standard spin echo sequences [29, 30], which add an extra π-pulse ($t_\pi = \pi/\Omega$) in the middle of the free evolution window τ. These sequences help to refocus the atomic state and reverse the inhomogeneous dephasing during the free evolution time, resulting in a much slower decay of the Ramsey contrast. With these sequences, we obtain $T_2 = 480(21)\,\mu$s for the stretched state of our qubits.

In order to compare the coherence in this qubit with other systems [26, 31, 32], we perform a spin echo on the transition between magnetically insensitive Zeeman states, $5S_{1/2}$, $|F = 1, m_F = 0\rangle \leftrightarrow |F = 2, m_F = 0\rangle$ of our qubits as most of the other experiments were also probing this magnetically insensitive Zeeman state coherence. Using the same procedure, we find the coherence time of the magnetically insensitive qubit to be $T_{2,c} = 9.5(6)$ ms, which is 20 times longer compared to the stretched state coherence [Fig. 3]. This observation is consistent with previous experiments with the superposition of magnetically insensitive Zeeman state in a red detuned dipole trap, which has a typical coherence time of 10 ms. It has been shown that the coherence time can be improved to tens of milliseconds by reducing the trap depth [26, 32]. The coherence time on the order of hundreds of milliseconds has also been demonstrated by reducing the differential light shift with a magic-intensity trapping technique [33]. We suspect that the fluctuations in dipole beam intensity gives rise to the differential light shift that limits our coherence time in the magnetic insensitive states. To confirm our hypothesis, the coherence time for magnetic insensitive states is calculated analytically following [26]. For the inhomogeneous dephasing caused by the energy-dependent differential light shift, we would expect $T_2^* = 0.97(2U_0)/(\delta k_B T_{atom}) \simeq 1.4\,$ms, using the measured trap depth $U_0 = k_B \times 0.88\,$mK and an infered maximum differential light shift $\delta \simeq 2\pi \times 13\,$kHz for our 851-nm FORT. An irreversible dephasing dominated by power fluctuations ΔP of the dipole laser with a measured Allan deviation $\Delta P_{\rm rms}/P = 0.66\,\%$ gives $T_2 = 1/(\delta\sigma_A) \simeq 20\,$ms.

IV. PERIODIC DD

In the previous section, we showed that the spin-echo technique, as the simplest example of DD with one single π-pulse, can already improve the coherence time. To understand the effect of more complex DD on coherence, we adapt a semiclassical picture in the context of nuclear-magnetic-resonance (NMR) systems, which classifies decoherence processes into two classes: longitudinal energy relaxation and transverse dephasing, due to random fields imparted by the environment.

The longitudinal relaxation process, described by a characteristic energy relaxation time T_1, is generally much slower than the transverse dephasing. Transverse dephasing involves the accumulation of random phases, which is the dominant factor that decreases the state coherence $W(\tau) = e^{-\chi(\tau)}$ after a duration τ [34].

Applying the control π-pulses flips the sign of the accumulated random phases in different periods alternatively. To qualitatively understand the efficiency of multipulse sequences on dephasing suppression, we focus on the change in the state coherence integral $\chi(\tau)$. For a state initialized in the equatorial plane of the Bloch sphere, we can write

$$\chi(\tau) = \frac{2}{\pi}\tau^2 \int_0^\infty S(\omega) g_N(\omega, \tau) d\omega, \qquad (1)$$

where $g_N(\omega, \tau)$ can be viewed as a frequency-domain filter function of the random phases for a refocusing sequence consisting of N π-pulses, and $S(\omega)$ is the power spectral density of environmental noise in the semiclassical picture, representing ensemble-averaged phase accumulated between the qubit states. Figure 4 illustrates the filter properties of function $g_N(\omega, \tau)$ for the Uhrig dynamical decoupling (UDD) sequence and periodic dynamical decoupling (PDD) sequence. For a fixed free evolution time τ, the filter function's peak frequency shifts higher as N increases, leading to a reduction of integrated low-frequency noise. The filter function gets narrower and is centered closer to $\omega = N\pi/\tau$ as N increases.

As a proof of concept, we first apply the simplest pulsed DD scheme, PDD sequence [34, 50]. Figure 5 shows the coherence evolution of the qubit system under the PDD sequence. In contrast to a monotonic decaying profile, we observe that the decaying envelopes contain collapses which always occur at the same partition period τ/N for various N. This can be explained by the atomic motion in the dipole trap, which has also been observed in previous studies [35, 36]; we discuss this further in the next section.

To compare various decaying envelopes, we define the coherence time T_2 as the time for the state coherence to decay by a factor of $1/e$. This is consistent with the usual definition in a bare two-level system. Figure 6 shows the coherence time as a function of number of π-pulses. The coherence time increases with the number N of π-pulses in a sequence. Our measurements suggest that the noise follows a $1/\omega^\alpha$ spectrum with $\alpha > 0$. The dependence of T_2 on N suggests that T_2 can potentially be further improved by using additional rephasing pulses. A similar trend has been observed in other qubit systems, including single silicon-vacancy centers [37], single nitrogen-vacancy centers [19], and single ^{43}Ca$^+$ ion system [38]. In our system, we are currently limited to pulse sequences with $N \leq 20$ as the contrast of the coherence evolution drops as N increases. This is because pulse imperfections including errors in the flip angles and finite pulse width introduce dephasing to the qubit, as discussed in [39]. More robust pulse sequences with pulse phases that are
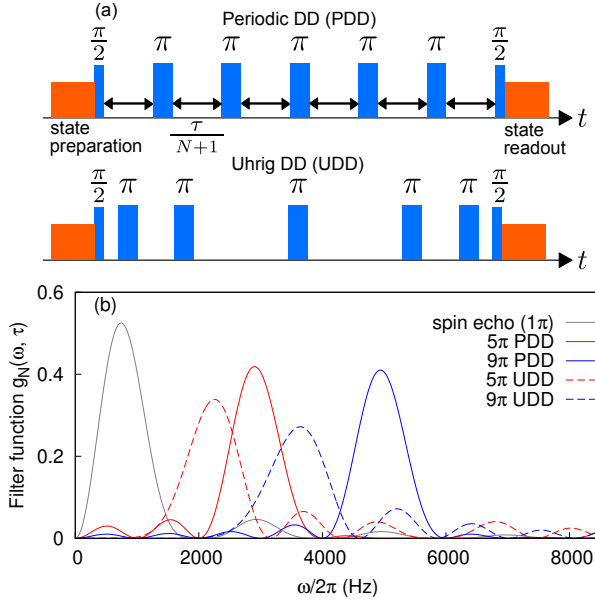
FIG. 4. (a): Schematic representation of various DD sequences. The qubit state is initialized in the $|\uparrow\rangle$ state. We then bring the qubit state to the superposition state $(|\uparrow\rangle + i|\downarrow\rangle)/\sqrt{2}$ with a $\pi/2$-pulse and let it evolve freely for a period τ, with τ being partitioned into small windows using π-pulses. PDD partitions τ into uniform periods. UDD has its j-th π-pulse locating at $\delta_j\tau$ with $\delta_j = \sin^2[\pi j/(2N+2)]$. (b): Filter function $g_N(\omega, \tau)$ for different pulse sequences. Increasing the number N of π-pulses shifts the peak to higher frequencies.

shifted appropriately can be applied to mitigate the pulse errors. Nevertheless, the preliminary refocusing strategy here has offered us an insight into the dephasing mechanism of a magnetic-sensitive qubit state.

In fact, the physical bound is $T_2 \leq T_1$ with the energy-relaxation time T_1 determined to be on the order of a second in our system.

To validate our findings, we simulate $\chi(\tau)$ under a simple noise model consisting of a $1/\omega^\alpha$ and a Gaussian centered at the axial trap frequency $\omega_0 = 2\pi \times 12.0\,\text{kHz}$. The $1/\omega^\alpha$ spectrum represents the noise floor produced by ambient magnetic field fluctuations and power fluctuations of the dipole light field. The Gaussian spectrum represents the differential light shift due to the atomic motion in an inhomogenous dipole light field. Our heuristic noise model is able to predict the recurring features as shown in Figure 5. We further test our model by comparing the coherence time T_2 for different numbers N of π-pulses [Figure 6]. Again, the model is in excellent agreement with the experimental data.

The qubit's sensitivity to the external magnetic field is $21\,\text{GHz/T}$ at low fields. Due to the high magnetic sensitivity of the qubit states, fluctuations in magnetic fields can be the dominant factor in the dephasing mechanism. To verify this, we have measured a r.m.s. magnetic field fluctuations of $19\,\text{nT}$ dominated by components at $50\,\text{Hz}$
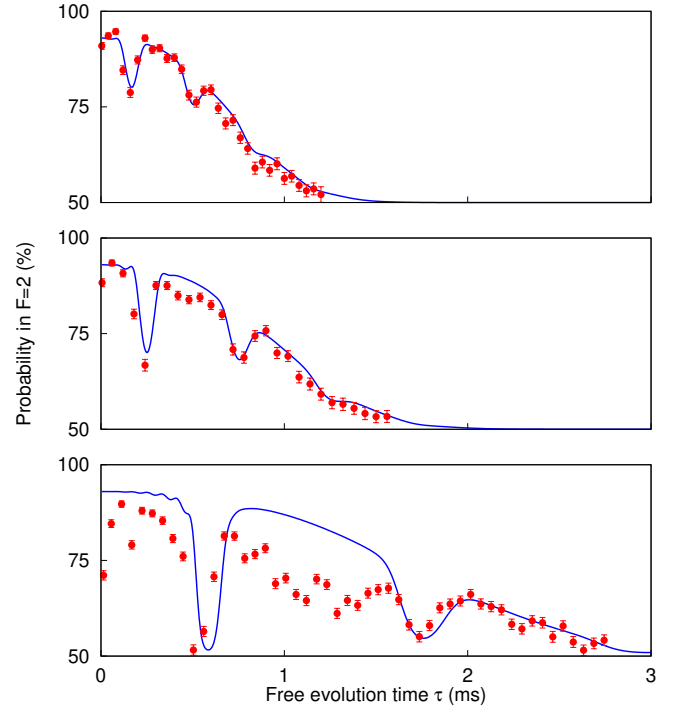

FIG. 5. Coherence evolution under Periodic DD (PDD) for $N = 3$ (top), $N = 5$ (middle), and $N = 13$ (bottom) π-pulses. Solid lines are numerical simulations using our heuristic noise model. Error bars represent standard error of binomial statistics accumulated from 300 repeated sequences.
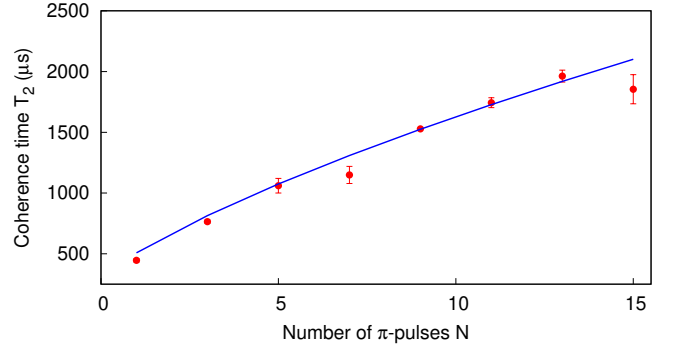

FIG. 6. Coherence time T_2 as a function of the number N of π-pulses. The solid line shows the simulation result for a spectrum $S(\omega) \propto 1/\omega^\alpha$ with $\alpha = 1.73$.

using a fluxgate magnetometer. We describe the accumulated phase due to magnetic noise during the free evolution of the Bloch vector as

$$\Phi(\tau, \phi) = \int_0^\tau \frac{\mu}{\hbar} B_\phi(t) dt, \qquad (2)$$

with $B_\phi(t)$ modelled as a $50\,\text{Hz}$ sinusoidal function with a phase ϕ. The coherence $W = \langle \cos\Phi(\tau, \phi)\rangle_\phi$ following [26], corresponds to a Ramsey coherence time T_2^* of $43\,\mu\text{s}$, in agreement with our observation.
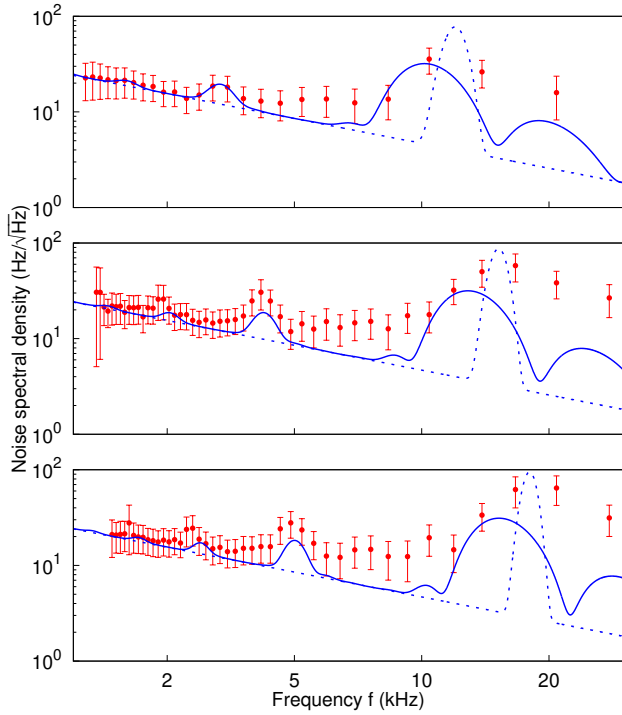
FIG. 7. Noise spectroscopy with DD adapted from atomic magnetometry. Red circle: noise spectral density reconstructed with experimental data. The recurring peaks are the feature of the filter function $g_N(\omega)$. Blue dashed line: noise spectrum of our heuristic noise model. Blue solid line: reconstructed noise spectral density in simulation. This is obtained by modulating the exact noise spectrum (blue dashed line) with the filter function of the chosen DD sequence. Trap depth is set to be 0.88 mK (top), 1.04 mK (middle) and 1.41 mK (bottom), respectively. The trap frequencies used in simulation are 12.0 kHz, 15.2 kHz, and 18.0 kHz, respectively.

Dynamical decoupling is also implemented in the field of magnetometry to reconstruct the noise spectrum [40, 41]. We manipulate the band-pass filter properties of $g_N(\omega, \tau)$ function to characterize the noise spectrum [42, 43]. Knowing that the filter function behaves as periodic sinc-shaped peaks at frequency $\omega_l \simeq (2l + 1)\omega$ with $\omega \simeq N\pi/\tau$, we probe the noise spectral density by varying N and τ.

Figure 7 shows the noise spectra probed experimentally when the dipole beam power is being varied. The reconstruction of noise spectral density $S(\omega)$ follows [42, 43]. The frequency range is determined by the choice of free evolution time τ. We observe the maximum noise density around 10.4 kHz, 16.7 kHz, and 20.8 kHz for dipole trap with trap depth of 0.88 mK, 1.04 mK, and 1.41 mK, respectively. As the dipole beam power increases, the maximum noise density shifts to higher frequencies. The noise peaking at the axial trap frequency can be explained by the polarization gradients of a tightly focused FORT following [44]. Around the focal plane, the tight focusing of FORT results in a spatially varying vector light shift of the qubit states. As the trap frequency

along axial direction $\omega_z = \sqrt{2U_0/(mz_R^2)}$ increases along with the trap depth U_0, the light shift noise due to oscillatory atomic motion shifts to higher frequencies.

We also observe recurring peaks in the noise spectra at lower frequencies. These peaks are the feature of the filter function $g_N(\omega)$, determined by the DD sequence. We numerically construct the noise spectral density modulated by the filter function with our heuristic noise model and find that the simulation predicts the recurring features well. By using the higher harmonics of the filter function, the trap frequency can be resolved with higher precision. We can use this as a basis for the precision measurement of trap parameters.

Another observation is that the width of the Gaussian noise in our model is much narrower than the noise spectral density modulated with a filter function. This is because the bandwidth of the filter function is inversely proportional to N. In our experiment, the number of refocusing pulses N used is less than 20, yielding a bandwidth that is comparable to the width of the Gaussian noise which we would like to resolve. It is possible to improve the resolution of the noise spectral density by increase the number of π-pulses N; however, there is a trade-off for increasing noise due to pulse errors.

Aside from the peak features, we notice that the background noise floor does not vary with dipole beam power. We measure the intensity fluctuation of the dipole beam and find that it only corresponds to noise spectral density of $0.5 \, \mathrm{Hz}/\sqrt{\mathrm{Hz}}$. This suggests that the background could be due to stray magnetic field fluctuation.

V. DD BENCHMARKING

We also apply Uhrig DD (UDD) protocols [45] to suppress dephasing in our qubit system. The UDD sequence has been analytically shown to provide strong suppression of phase accumulation when the noise environment contains a high-frequency component and a sharp high-frequency cutoff. The π-pulse sequence and the characteristics of the filter function $g_N(\omega, \tau)$ for UDD are shown in Figure 4. A feature of UDD is the lack of higher harmonics but more side lobes. Compared with the PDD protocol having the same number of π-pulses N, UDD produces a pass band with a larger width peaking at a lower frequency. This indicates that UDD could perform worse under a broadband noise spectrum.

Figure 8 shows the UDD coherence evolution of a single atom qubit. Again, the simulation with our heuristic noise model introduced in Sec. IV predicts the wiggles qualitatively in the $|\uparrow\rangle$ population as the total free evolution time τ varies. However, the simulation falls short in predicting the magnitude of the wiggles. This is most likely due to the simplified formulation for the filter function $g_N(\omega, \tau)$ that assumes an instantaneous π-pulse.

We also look at the $1/e$ coherence time under the UDD protocol for a free evolution time τ larger than $500 \, \mu s$ to minimize the influence from the wiggles. We observe
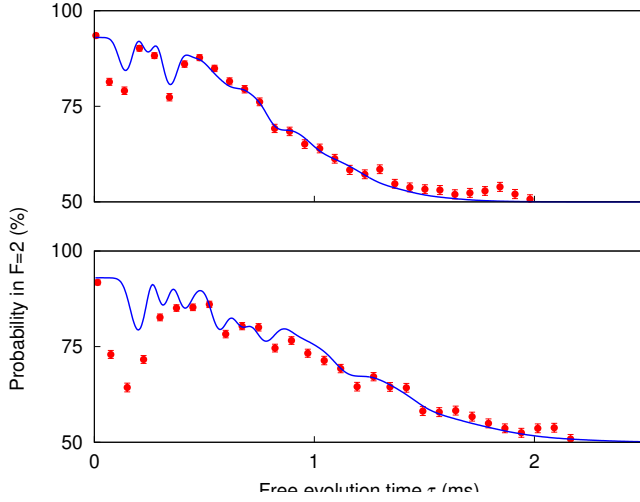
FIG. 8. Implementing Uhrig dynamic decoupling (UDD). Top: UDD with 3 π-pulses, $T_2 = 926\,\mu s$. Bottom: UDD with 5 π-pulses, $T_2 = 1285\,\mu s$. Solid lines are numerical simulations using our heuristic noise model with the same parameters implemented in section IV. Error bars represent standard error of binomial statistics accumulated from 300 repeated sequences.

a coherence time of $926\,\mu s$ and $1285\,\mu s$ for $N = 3$ and $N = 5$ π-pulses, respectively. Compared with the coherence time obtained using PDD with the same number of π-pulses ($764\,\mu s$ for $N = 3$ and $1060\,\mu s$ for $N=5$), we observe an improvement of $21.2\,\%$ on the coherence time, consistent for both $N = 3$ and $N = 5$. We also notice that PDD and UDD sequences perform quite similarly because in general a DD sequence requires a rather distinctive noise spectrum to outperform the others.

For most applications in quantum information processing, we aim to preserve coherence maximally for a given duration. We demonstrate the optimization protocol with $N = 5$ π-pulses. As shown in Figure 9 (a), we impose a fixed free evolution time τ and reflection symmetry as constraints to reduce the number of free parameters from 6 to 2. To better understand the effect of the noise on the qubit coherence, we numerically calculate the dynamics of the qubit state using our heuristic noise model introduced in previous sections, following Eqn. (1).

We find a good agreement between the observed coherence and the model for the same parameters used in the previous section. The maximum coherence is obtained with the protocol that follows $\left(\frac{\tau_0}{\tau}, \frac{\tau_1}{\tau}, \frac{\tau_2}{\tau}\right) = (11.2\,\%, 19.2\,\%, 19.6\,\%)$. This optimal sequence matches well with the Carr-Purcell (CP) sequence, which is widely used in the field of NMR and is constructed with the first and last precession periods are half of the duration of the interpulse period, e.g. $\left(\frac{\tau_0}{\tau}, \frac{\tau_1}{\tau}, \frac{\tau_2}{\tau}\right) = (10\,\%, 20\,\%, 20\,\%)$ [46, 49]. We would like to point out that in this discussion we are only looking at the coherence of one single state possessing a particular phase. For an arbitrary state on the Bloch sphere, more robust sequences such as KDD_x and KDD_{xy} are more effective in preserving the qubit
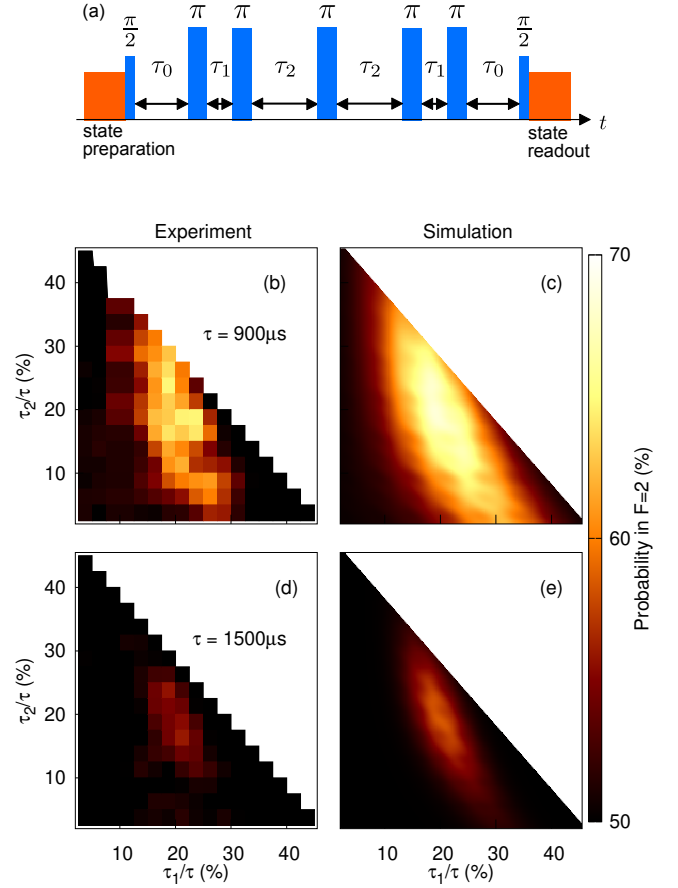
FIG. 9. Optimization with five π-pulses for a fixed free evolution time $\tau = 900\,\mu s$ and $\tau = 1500\,\mu s$. (a): Schematic representation of the DD sequence, satisfying $\tau_0 + \tau_1 + \tau_2 = 0.5\tau$. (b-d): Population of $F = 2$ state at the end of refocusing. For both $\tau = 900\,\mu s$ and $\tau = 1500\,\mu s$, the maximum fidelity is not given by standard DD sequences such as UDD ($\tau_1/\tau = 18.3\,\%$, $\tau_2/\tau = 25.0\,\%$) or PDD ($\tau_1/\tau = 16.7\,\%$, $\tau_2/\tau = 16.7\,\%$), the maximal point locates at $\tau_1/\tau = 19.2\,\%$, $\tau_2/\tau = 19.6\,\%$ in the simulation.

coherence [39, 47].

VI. CONCLUSION

We have presented a detailed experimental study of the implementation of dynamical decoupling (DD) in a single neutral atom qubit system. In addition to the performance comparison between two standard DD protocols, periodic DD and Uhrig DD, we find an improvement in the coherence time T_2 by two orders of magnitude from T_2^*. The observed coherence time of $2\,ms$ is sufficient to facilitate the high-fidelity transfer of quantum states between quantum repeater nodes separated by hundreds of kilometers [1]. In particular, we characterized the noise spectrum of an optically trapped Rubidium atom. We

demonstrated that the CP sequence performs the best in the longer timescale for sequences with refocusing pulses of the same phase.

Future experiments will explore lowering the noise floor and motion-dependent dephasing. Improvements will extend the coherence times and hence open up new possibilities for the implementation of more robust free-space neutral atom quantum memories for future quantum repeater networks [48]. A better understanding of the qubit response to noise may also help to develop a broadband single-atom sensor which would allow to image magnetic fields with a spatial resolution at atomic length scales.

Optimization with a larger number of rephasing pulses may also further increase the qubit coherence time with the implementation of rebust refocusing sequences.

[1] L. Childress, J. M. Taylor, A. S. Sørensen, and M. D. Lukin, Phys. Rev. Lett. **96**, 070504 (2006).

[2] H. J. Kimble, Nature **453**, 1023 (2008).

[3] A. Reiserer, N. Kalb, G. Rempe, and S. Ritter, Nature **508**, 237 (2014).

[4] J. Volz, M. Weber, D. Schlenk, W. Rosenfeld, J. Vrana, K. Saucke, C. Kurtsiefer, and H. Weinfurter, Phys. Rev. Lett. **96**, 030404 (2006).

[5] M. K. Tey, G. Maslennikov, T. C. H. Liew, S. A. Aljunid, F. Huber, B. Chng, Z. Chen, V. Scarani, and C. Kurtsiefer, New J. Phys. **11**, 043011 (2009).

[6] E. Vetsch, D. Reitz, G. Sagué, R. Schmidt, S. T. Dawkins, and A. Rauschenbeutel, Phys. Rev. Lett. **104**, 203603 (2010).

[7] L. Alber, M. Fischer, M. Bader, K. Mantel, M. Sondermann, and G. Leuchs, J. Eur. Opt. Soc.-Rapid Publ. **13**, 14 (2017).

[8] M. K. Bhaskar, D. D. Sukachev, A. Sipahigil, R. E. Evans, M. J. Burek, C. T. Nguyen, L. J. Rogers, P. Siyushev, M. H. Metsch, H. Park, F. Jelezko, M. Lončar, and M. D. Lukin, Phys. Rev. Lett. **118**, 223603 (2017).

[9] N. H. Lindner and T. Rudolph, Phys. Rev. Lett. **103**, 113602 (2009).

[10] I. Schwartz, D. Cogan, E. R. Schmidgall, Y. Don, L. Gantz, O. Kenneth, N. H. Lindner, and D. Gershoni, Science **354**, 434 (2016).

[11] M. Steiner, Y.-S. Chin, and C. Kurtsiefer, New J. Phys. **21**, 023012 (2019).

[12] M. J. Biercuk, H. Uys, A. P. VanDevender, N. Shiga, W. M. Itano, and J. J. Bollinger, Nature **458**, 996 (2009).

[13] J. R. West, D. A. Lidar, B. H. Fong, and M. F. Gyure, Phys. Rev. Lett. **105**, 230503 (2010).

[14] G. de Lange, Z. H. Wang, D. Riste, V. V. Dobrovitski, and R. Hanson, Science **330**, 60 (2010).

[15] A. M. Souza, G. A. Álvarez, and D. Suter, Phys. Rev. Lett. **106**, 240501 (2011).

[16] N. Timoney, I. Baumgart, M. Johanning, A. F. Varón, M. B. Plenio, A. Retzker, and C. Wunderlich, Nature **476**, 185 (2011).

[17] M. Lovrić, D. Suter, A. Ferrier, and P. Goldner, Phys. Rev. Lett. **111**, 020503 (2013).

[18] G. A. Paz-Silva, S. W. Lee, T. J. Green, and L. Viola, New J. Phys. **18**, 073020 (2016).

[19] D. D. Sukachev, A. Sipahigil, C. T. Nguyen, M. K. Bhaskar, R. E. Evans, F. Jelezko, and M. D. Lukin, Phys. Rev. Lett. **119**, 223602 (2017).

[20] Y.-S. Chin, M. Steiner, and C. Kurtsiefer, Nat. Comm. **8**, 1200 (2017).

[21] Y.-S. Chin, M. Steiner, and C. Kurtsiefer, Phys. Rev. A **96**, 033406 (2017).

[22] A. Fuhrmanek, R. Bourgain, Y. R. P. Sortais, and A. Browaeys, Phys. Rev. Lett. **106**, 133003 (2011).

[23] M. J. Gibbons, C. D. Hamley, C.-Y. Shih, and M. S. Chapman, Phys. Rev. Lett. **106**, 133002 (2011).

[24] W. Rosenfeld, J. Volz, M. Weber, and H. Weinfurter, Phys. Rev. A **84**, 022343 (2011).

[25] S. Kuhr, W. Alt, D. Schrader, I. Dotsenko, Y. Miroshnychenko, W. Rosenfeld, M. Khudaverdyan, V. Gomer, A. Rauschenbeutel, and D. Meschede, Phys. Rev. Lett. **91**, 213002 (2003).

[26] S. Kuhr, W. Alt, D. Schrader, I. Dotsenko, Y. Miroshnychenko, A. Rauschenbeutel, and D. Meschede, Phys. Rev. A **72**, 023406 (2005).

[27] M. F. Andersen, A. Kaplan, and N. Davidson, Phys. Rev. Lett. **90**, 023001 (2003).

[28] M. F. Andersen, A. Kaplan, T. Grünzweig, and N. Davidson, Phys. Rev. A **70**, 013405 (2004).

[29] E. L. Hahn, Phys. Rev. **80**, 580 (1950).

[30] L. M. K. Vandersypen and I. L. Chuang, Rev. Mod. Phys. **76**, 1037 (2005).

[31] D. D. Yavuz, P. B. Kulatunga, E. Urban, T. A. Johnson, N. Proite, T. Henage, T. G. Walker, and M. Saffman, Phys. Rev. Lett. **96**, 063001 (2006).

[32] M. P. A. Jones, J. Beugnon, A. Gaëtan, J. Zhang, G. Messin, A. Browaeys, and P. Grangier, Phys. Rev. A **75**, 040301(R) (2007).

[33] J. Yang, X. He, R. Guo, P. Xu, K. Wang, C. Sheng, M. Liu, J. Wang, A. Derevianko, and M. Zhan, Phys. Rev. Lett. **117**, 123201 (2016).

[34] M. J. Biercuk, A. C. Doherty, and H. Uys, J. Phys. B **44**, 154002 (2011).

[35] G. Afek, J. Coslovsky, A. Mil, and N. Davidson, Physical Review A **96**, 043831 (2017).

[36] S. B. Markussen, J. Appel, C. Østfeldt, J.-B. S. Béguin, E. S. Polzik, and J. H. Müller, Applied Physics B: Lasers and Optics **126**, Art (2020).

[37] C. A. Ryan, J. S. Hodges, and D. G. Cory, Phys. Rev. Lett. **105**, 200402 (2010).

[38] D. J. Szwer, S. C. Webster, A. M. Steane, and D. M. Lucas, J. Phys. B **44**, 025501 (2010).

[39] M. A. A. Ahmed, G. A. Álvarez, and D. Suter, Physical Review A **87**, 042309 (2013).

[40] M. Hirose, C. D. Aiello, and P. Cappellaro, Phys. Rev. A **86**, 062320 (2012).

[41] I. Baumgart, J.-M. Cai, A. Retzker, M. B. Plenio, and C. Wunderlich, Phys. Rev. Lett. **116**, 240801 (2016).

[42] J. Bylander, S. Gustavsson, F. Yan, F. Yoshihara, K. Harrabi, G. Fitch, D. G. Cory, Y. Nakamura, J. S. Tsai, and W. D. Oliver, Nat. Phys. **7**, 565 (2011).

[43] S. Hernández-Gómez, F. Poggiali, P. Cappellaro, and N. Fabbri, Phys. Rev. B **98**, 214307 (2018).

[44] J. D. Thompson, T. G. Tiecke, A. S. Zibrov, V. Vuletić, and M. D. Lukin, Phys. Rev. Lett. **110**, 133001 (2013).

[45] G. S. Uhrig, Phys. Rev. Lett. **98**, 100504 (2007).

[46] C. P. Slichter, *Principles of Magnetic Resonance* (Springer Berlin Heidelberg, 1990).

[47] A. Ajoy, G. A. Álvarez, and D. Suter, Physical Review A **83**, 032303 (2011).

[48] M. Razavi, M. Piani, and N. Lütkenhaus, Phys. Rev. A **80**, 032301 (2009).

[49] S. Pasini and G. S. Uhrig, Phys. Rev. A **81**, 012309 (2010).

[50] G. A. Álvarez, A. Ajoy, X. Peng, and D. Suter, Phys. Rev. A **82**, 042306 (2010).